Electronic Supplementary Material (ESI) for New Journal of Chemistry.

Supporting Information

A Carboxylate- and Pyridine-based Organic Anode Material for K-ion Batteries

Kathryn Holguin,[a] Kaiqiang Qin,[a] Jinghao Huang,[a] Chao Luo,*[a,b]

[a]Department of Chemistry and Biochemistry, George Mason University, Fairfax, VA, 22030, USA

[b]Quantum Science & Engineering Center, George Mason University, Fairfax, VA, 22030, USA

*Corresponding author: cluo@gmu.edu

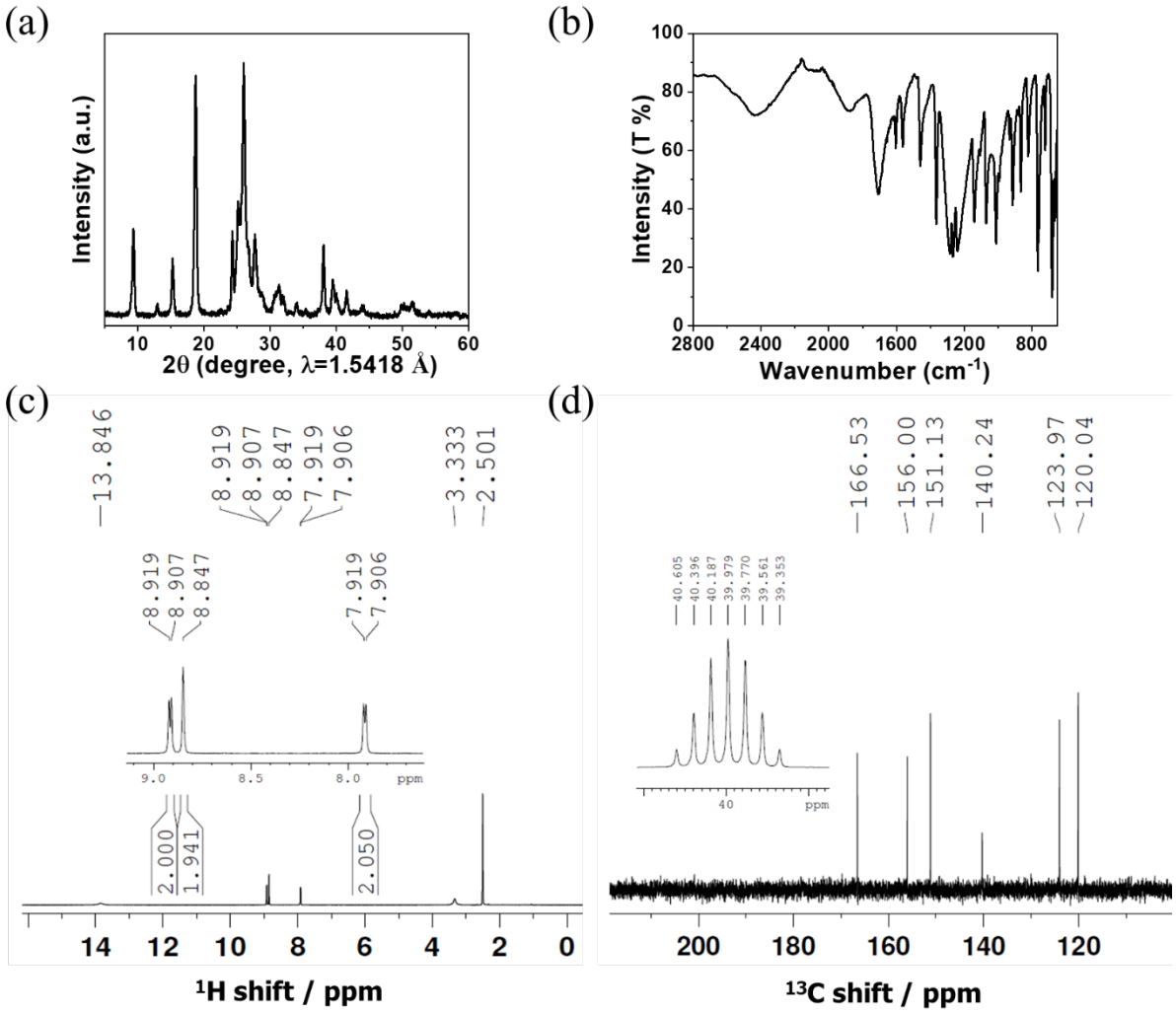

Figure S1. Material characterizations of 2,2'-bypyridine-4,4'-dicarboxylic acid (precursor material for K-DCA). (a) PXRD pattern; (b) FTIR spectrum; (c) ^{1}H NMR spectrum with $DMSOd_6$ peak at ~2.5 ppm and H_2O peak at ~3.3 ppm; (d) ^{13}C NMR spectrum with $DMSOd_6$ peak at ~40 ppm.

The ^{1}H NMR spectrum shows three peaks in the range from ~7.9-8.9 ppm representing the protons in the pyridine moieties of the Precursor, while the peak at 13.846 ppm represents protons in the carboxylic acid moiety. There is an obvious peak at 2.501 ppm, corresponding to the chemical shift of H in the $DMSOd_6$ solvent, and a peak at 3.333 ppm corresponding to the chemical

shift of H in the ethanol used for cleaning the tubes. The ^{13}C NMR spectrum shows three peaks at 120.04 ppm, 123.97 ppm, and 140.24 ppm corresponding to sp^2 carbons in the pyridine ring bonded with protons. The ^{13}C NMR peak at 151.13 ppm corresponding to sp^2 carbons in the pyridine ring bonded to the carboxylate groups, while the peak at 156.00 ppm corresponding to sp^2 carbons in the pyridine rings bonded to each other, and the ^{13}C NMR peak at 166.53 ppm corresponding to sp^2 carbons in the carboxylate groups. There is an obvious peak (septet) at ~40 ppm, corresponding to the chemical shift of C in $DMSOd_6$ solvent.

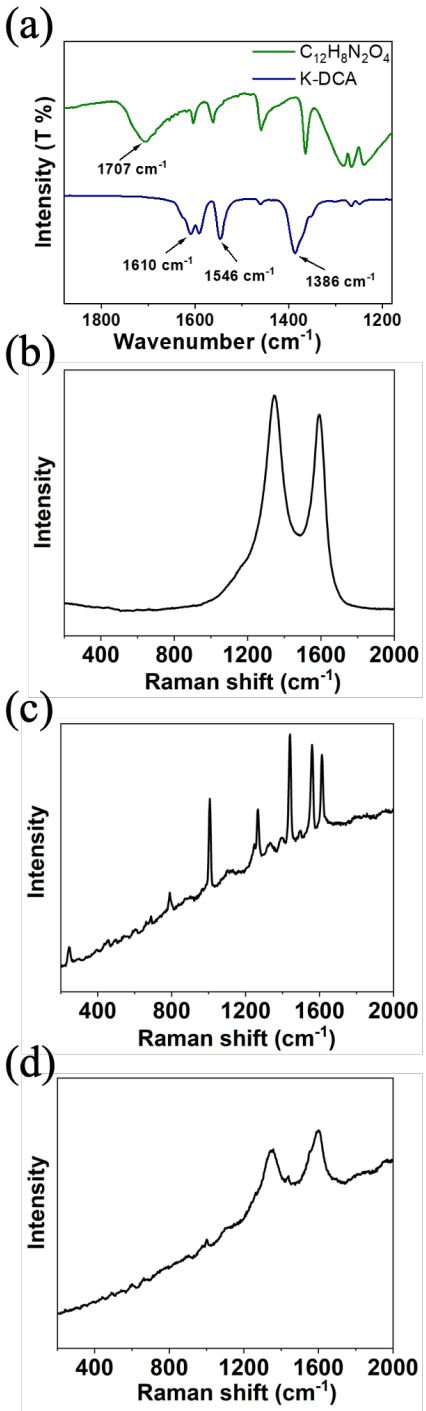

Figure S2. (a) Enlargement of FTIR of 2,2'-bypyridine-4,4'-dicarboxylic acid ($C_{12}H_8N_2O_4$) and 2,2'-bypyridine-4,4'-dicarboxylic acid dipotassium salt (K-DCA) showing newly formed peaks resulting from complete conversion of dicarboxylic acid to potassium carboxylate salt; Raman spectra for (b) NrGO, (c) K-DCA, (d) the K-DCA-NrGO composite.

Newly formed peaks can be observed at 1610 cm^{-1} and 1386 cm^{-1}, corresponding to the asymmetrical and symmetrical vibrations of C=O in the carboxylates, respectively, while the peak at 1546 cm^{-1} corresponds to the vibrations of C=N in the pyridine moieties of K-DCA.

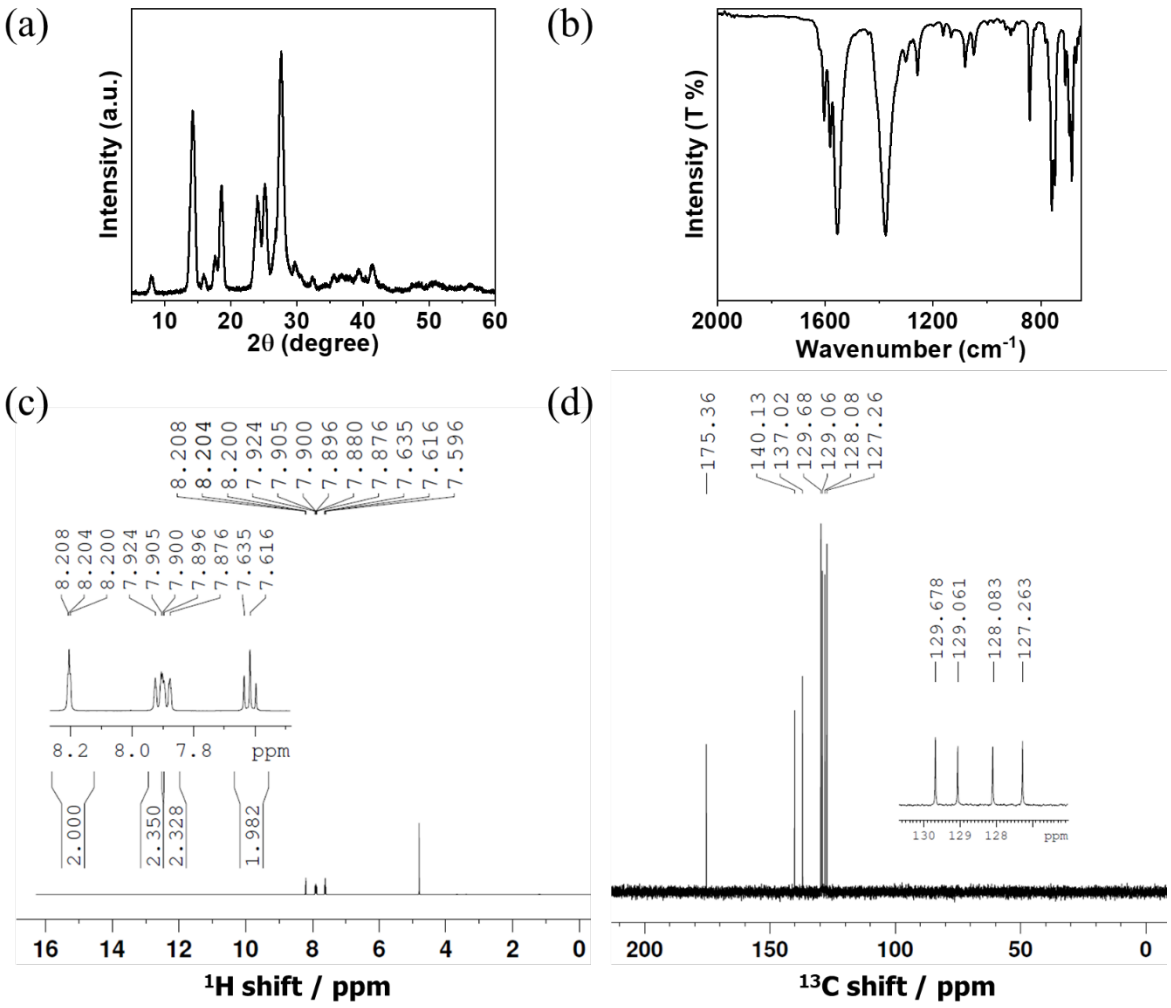

Figure S3. Material characterizations of biphenyl-3,3'-dicarboxylic acid dipotassium salt ($K_2C_{14}H_8O_4$). (a) PXRD pattern; (b) FTIR spectrum; (c) ^{1}H NMR spectrum with D_2O peak at 4.8 ppm; (d) ^{13}C NMR spectrum.

The ^{1}H NMR spectrum in Fig. S3c shows four peaks in the range from ~7.6-8.2 ppm (two peaks overlapping at 7.8 and 7.9 ppm), representing the protons in the biphenyl moieties of $K_2C_{14}H_8O_4$. There is an obvious peak at 4.8 ppm, corresponding to the chemical shift of H in the

D_2O solvent. The ^{13}C NMR spectrum in Fig. S3d shows four peaks at 127.26 ppm, 128.08 ppm, 129.06 ppm, and 137.02 ppm, corresponding to sp^2 carbons in the biphenyl ring bonded with protons, while the peak at 129.68 ppm corresponds to sp^2 carbons in the biphenyl ring bonded to the carboxylate groups. The ^{13}C NMR peak at 140.13 ppm corresponds to sp^2 carbons in the benzene rings bonded to each other, while the ^{13}C NMR peak at 175.36 ppm corresponds to sp^2 carbons in the carboxylate groups.

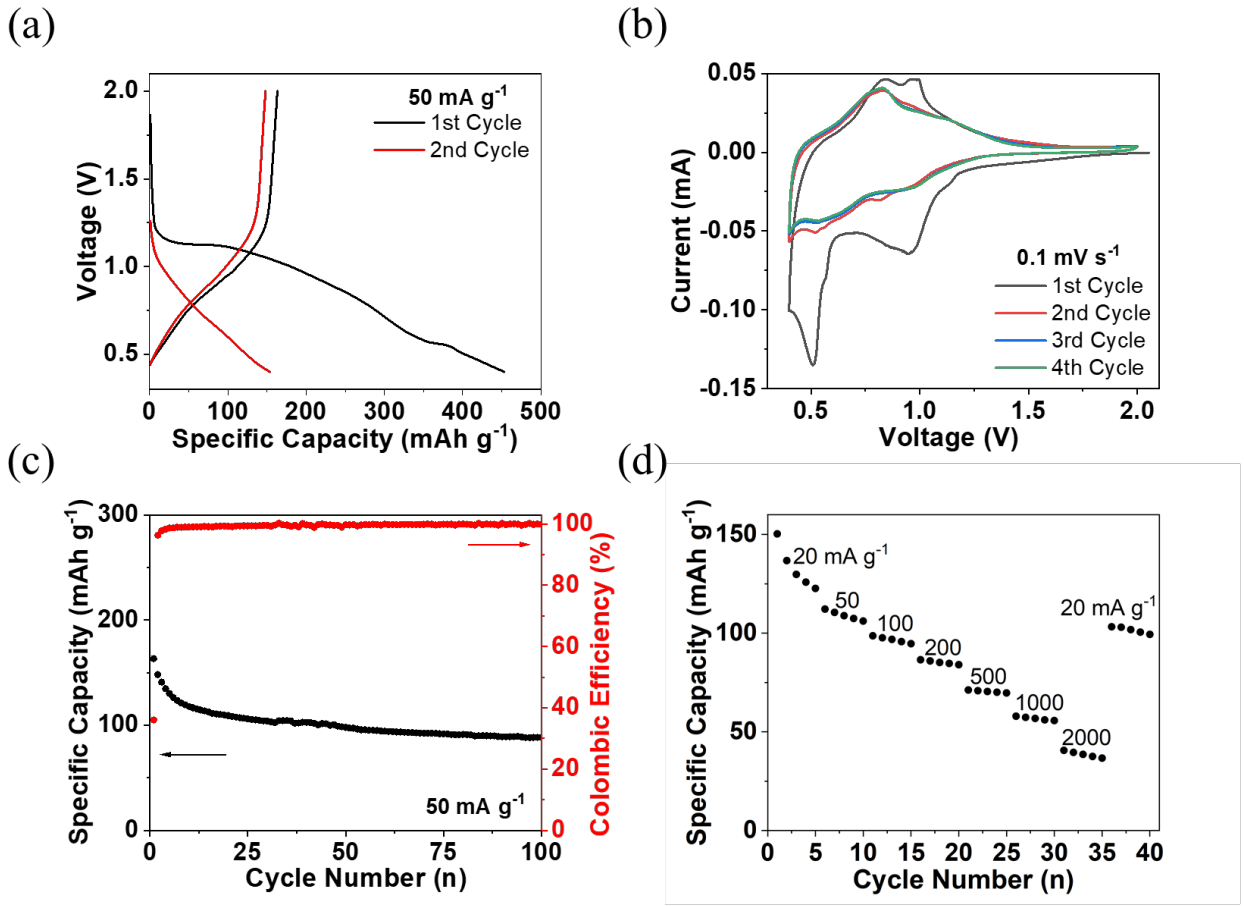

Figure S4. Electrochemical performance and reaction kinetics of K-DCA in KIBs. (a) Galvanostatic charge-discharge curves; (b) Cyclic voltammograms at 0.1 mV s^{-1}; (c) De-potassiation capacity and Coulombic efficiency versus cycle number at the current density of 50 mA g^{-1}; (d) Rate performance at various current densities.

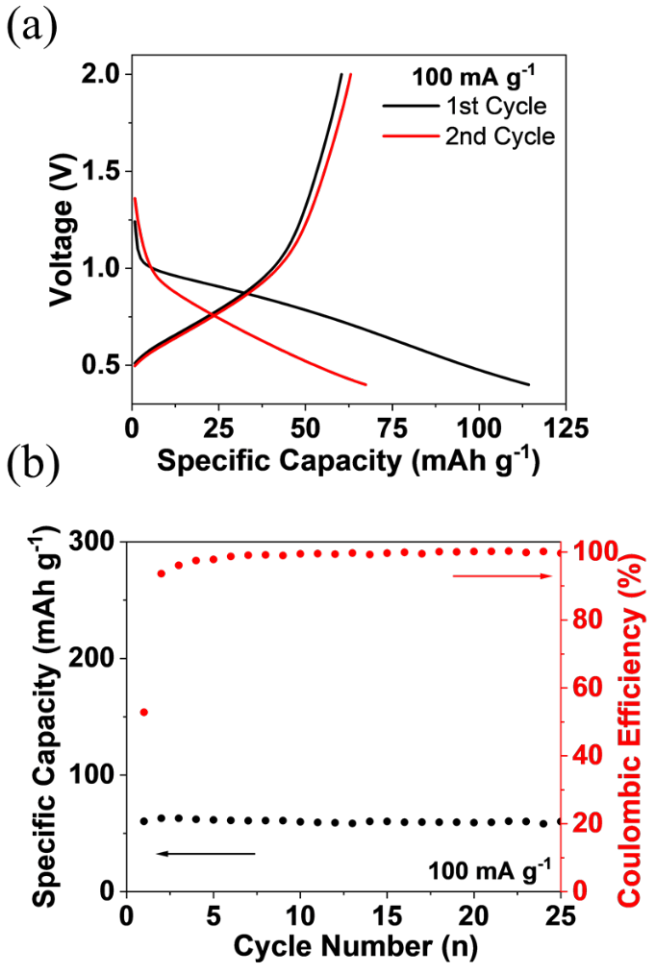

Figure S5. Electrochemical performance of Carbon Black in KIBs. (a) Galvanostatic charge-discharge curves; (b) De-potasiation capacity and Coulombic efficiency versus cycle number at a current density of 100 mA g^{-1}.

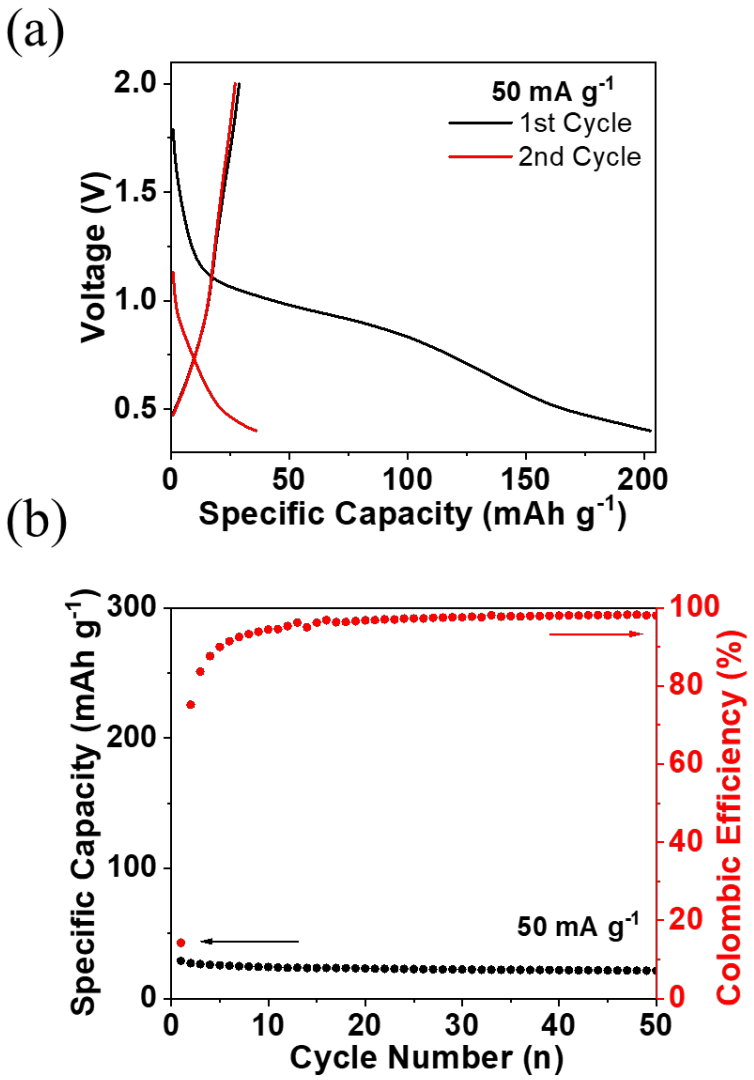

Figure S6. Electrochemical performance of biphenyl-3,3'-dicarboxylic acid dipotassium salt ($K_2C_{14}H_8O_4$) in KIBs. (a) Galvanostatic charge-discharge curves; (b) De-potassiation capacity and Coulombic efficiency versus cycle number at the current density of 50 mA g^{-1}.

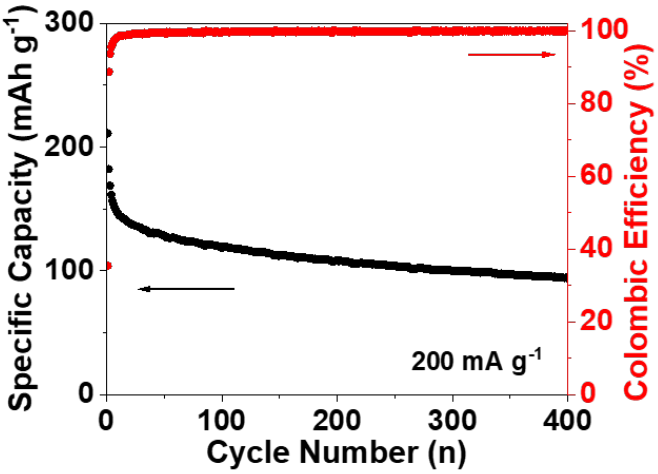

Figure S7. Electrochemical performance of K-DCA-NrGO in KIBs. De-potassiation capacity and Coulombic efficiency versus cycle number at the current density of 200 mA g^{-1}.

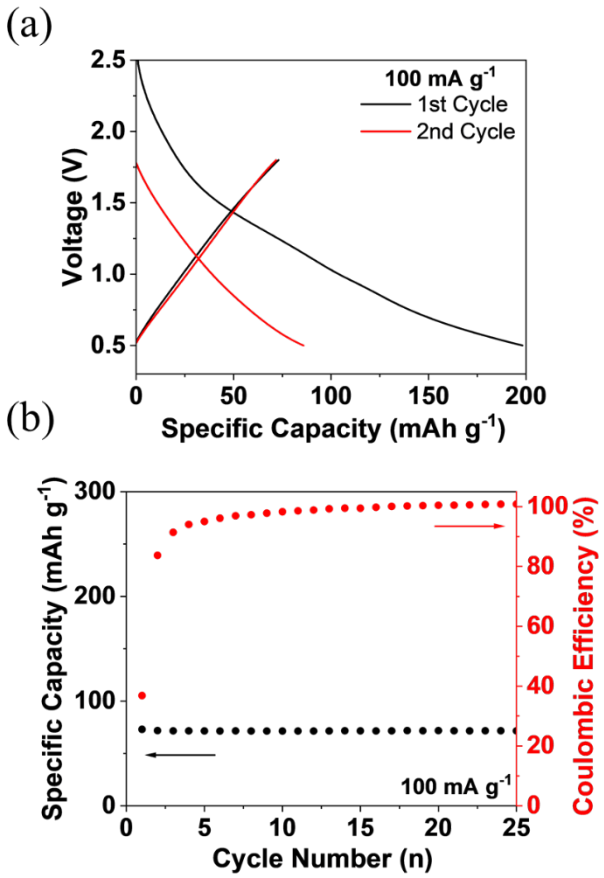

Figure S8. Electrochemical performance of Nitrogen-doped Reduced Graphene Oxide (NrGO) in KIBs. (a) Galvanostatic charge-discharge curves; (b) De-potassiation capacity and Coulombic efficiency versus cycle number at a current density of 100 mA g^{-1}.

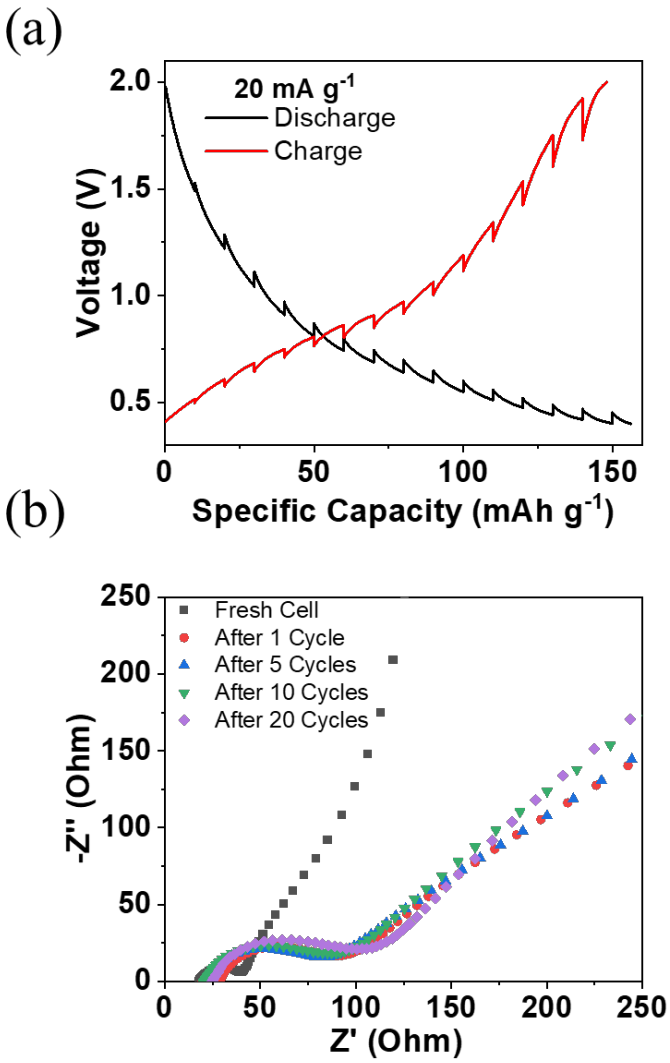

Figure S9. Reaction kinetics of K-DCA in KIBs. (a) Potential response during GITT measurements at 20 mA g^{-1}; (b) Impedance analysis before and after charge/discharge.

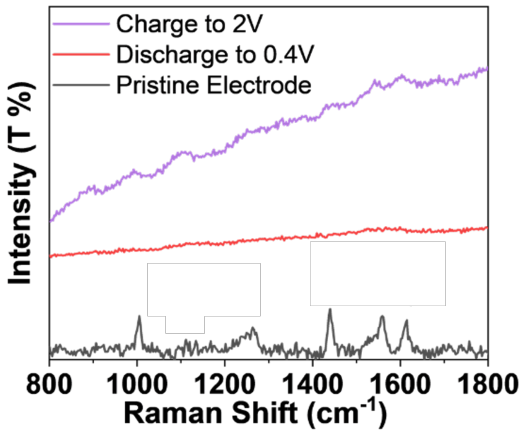

Figure S10. *ex-situ* Raman spectra of K-DCA demonstrating carbonyl and pyridine groups participating in four-electron/K^+ mechanism.

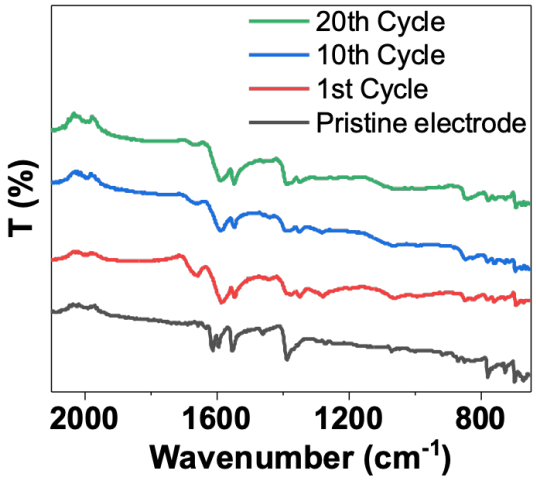

Figure S11. FTIR spectra of pristine and cycled K-DCA electrodes in KIBs.